Review of the Hierarchical Multi-Mode Molecular Stress Function Model for Broadly Distributed Linear and LCB Polymer Melts

Esmaeil Narimissa,[1,2] **Manfred H. Wagner**[3]
[1]*Department of Chemical Engineering, Technion–Israel Institute of Technology (IIT), Technion City, Haifa, 32 000, Israel*
[2]*Department of Chemical Engineering, Guangdong Technion–Israel Institute of Technology (GTIIT), Shantou, 515063, China*
[3]*Polymer Engineering/Polymer Physics, Berlin Institute of Technology (TU Berlin), Fasanenstrasse 90, 10623, Berlin, Germany*

We developed a novel Hierarchical Multi-mode Molecular Stress Function (HMMSF) model for linear and long-chain branched (LCB) polymer melts implementing the basic ideas of (1) hierarchical relaxation, (2) dynamic dilution, (3) interchain tube pressure, and (4) convective constraint release. With a minimum number of nonlinear free parameters and remarkable quantitative predictions of the rheology of polymer melts, this model is an outstanding option for the simulation of different processing operations in the polymer industry. The excellent predictions of this model were demonstrated in uniaxial, equibiaxial, and planar extensional deformations for linear and LCB melts, as well as in shear flow for a LCB polymer, with a minimum number of adjustable free nonlinear material parameters, that is, one in the case of extensional flows, and two in shear flow. In this contribution, we review the development of the HMMSF model and present a reduced number of well-defined constitutive relations comprising the rheology of both linear and LCB melts. We also extend the comparison of model and data to cover the shear flow of a linear polymer melt. POLYM. ENG. SCI., 9999:1–11, 2018.

INTRODUCTION

The extent of molecular weight distribution and long-chain branching of polymers has a significant impact on their rheological properties both in the linear and the non-linear viscoelastic regimes, and the onset and strength of the so-called strain-hardening behavior in extensional flows (i.e., the deviation from the linear viscoelastic envelope) occur faster and more accentuated in long-chain branched (LCB) melts as opposed to linear melts. Recent developments of quantitative rheological models relating molecular structures to flow properties and vice versa have seen considerable progress, albeit often at the cost of numerous model assumptions and adjustable material parameters. Attempts have been made of integrating the rheological modeling into the modeling of polymerization reactions and melt forming operations with the expectation of detailed information on the molecular structure of polymers, which in turn determines the linear and nonlinear rheological properties and the processing behavior of polymers (see e.g. [6]). Although there is some confidence in the rheological modeling of linear and LCB polymers in the linear-viscoelastic regime (see e.g. [7]), there is less agreement on the modeling of nonlinear viscoelasticity even for monodisperse systems.

The significance of the nonlinear viscoelastic rheological modeling of polydisperse polymeric systems for quantitative flow simulations in polymer processing has prompted us to develop a comprehensive constitutive model capable of predicting the rheological behaviors of linear and LCB polymers for various categories of flow that is, uniaxial extensional, multiaxial extensional, and shear deformations. Due to its reduced number of free nonlinear parameters (i.e., one in extensional flows and two in shear flow), mathematical simplicity/flexibility, and proven quantitative predictions of the rheological behaviors of polymeric melts, the HMMSF model is an excellent choice for finite element simulations of polymer processing techniques (e.g., injection modeling, extrusion, film blowing, fiber spinning, etc.), as well as free-surface deformations. The general guideline in the development of this model has been to recognize that the rheological effects of the complex (and in the case of LCB polymers often unknown) molecular structures are already contained in the linear-viscoelastic spectrum of relaxation times of the polymers, and that only a limited number of well-defined constitutive assumptions concerning the nonlinear rheology is needed, thereby, reducing the number of adjustable free nonlinear material parameters to a minimum. Although in principle the linear-viscoelastic relaxation modulus, which is the basis of the HMMSF model, could be obtained from molecular modeling or simulations, we prefer here to use spectra obtained by fitting experimentally determined linear-viscoelastic data.

In Narimissa et al. [1,2,5], we introduced the Hierarchical Multi-mode Molecular Stress Function (HMMSF) model for LCB polymers, which implements the basic ideas of the pom-pom model, hierarchal relaxation, dynamic dilution, and interchain tube pressure. We showed that this model accurately predicts the elongational and multiaxial extensional viscosity as well as the shear viscosity of several LCB polymer melts based exclusively on their linear-viscoelastic characterization. It features only a single non-linear material parameter, the so-called dilution modulus G_D, for extensional flows, and in addition a constraint release (CR) parameter for shear flow. In Narimissa and Wagner [3,4] we extended the HMMSF model to monodisperse, bidisperse, and polydisperse linear polymer melts by means of relating the relaxation times to the Rouse stretch-relaxation times for each relaxation mode.

The objectives of this contribution are to review the structure and predictions of the HMMSF model in extensional and shear deformations, and to present a reduced number of well-defined

Correspondence to: E. Narimissa; e-mail: esmaeiln@technion.ac.il or M. H. Wagner manfred.wagner@tu-berlin.de
DOI 10.1002/pen.24972
Published online in Wiley Online Library (wileyonlinelibrary.com).

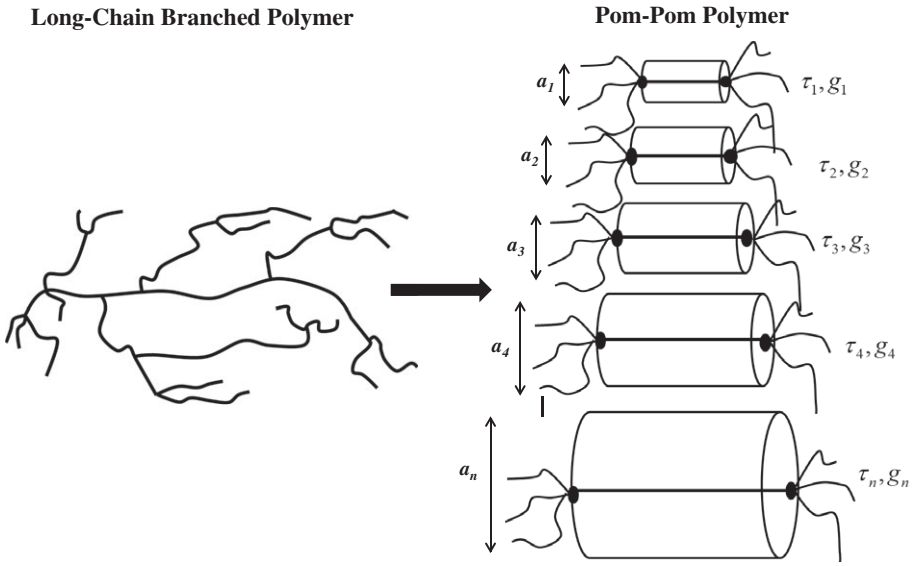

FIG. 1. Schematic representation of a LCB polymer by a hierarchical series of pom-pom polymers with $\tau_{i+1} > \tau_i$, and $a_1 < a_2 < \cdots < a_n$. For details see text. Reprinted from [4], Copyright (2016), with permission from Elsevier.

constitutive relations comprising the rheology of both linear and LCB melts. In addition, we discuss the predictions of the HMMSF model for shear flow of linear polymer melts, which has not been done previously.

THEORETICAL BACKGROUND

HMMSF Model

From the basic idea of the pom-pom model, an LCB polymer can be represented by a series of individual pom-pom macromolecules with two branch points, characterized by the parameters $\{\tau_i, g_i\}$ of a discrete relaxation spectrum [1]. Figure 1 displays a schematic illustration of the proposed conversion of an LCB macromolecule into a hierarchical series of pom-pom polymers, where the pom–poms with short relaxation times dynamically dilute those with longer relaxation times. As shown schematically, the tube diameter a_i and the contour length grow with increasing relaxation time, when the already relaxed pom–poms with shorter relaxation times dilute the ones with longer relaxation times.

In the case of linear polymers, similarly an ensemble of entangled linear chains is represented by a series of segments with hierarchically increasing tube diameters [3] (Fig. 2). Segments with tube diameter a_i are characterized by a relaxation time τ_i, and their entanglement fraction in the polydisperse melt is proportional to a partial relaxation modulus g_i. Segments with shorter relaxation times dilute the ones with longer relaxation times, thereby increasing the tube segment diameters a_i. In this way, through hierarchical relaxation mechanisms, segments with longer relaxation times are more diluted than segments with shorter relaxation times that is, the longer the segmental relaxation time τ_i, the more diluted is the specific segment.

The extra stress tensor of the HMMSF model [1] is given as,

$$\sigma(t) = \sum_i \int_{-\infty}^{+\infty} \frac{\partial G_i(t-t')}{\partial t'} f_i^2(t,t') \mathbf{S}_{DE}^{IA}(t,t') dt' \qquad (1)$$

Here $\mathbf{S}_{\mathrm{DE}}^{\mathrm{IA}}$ is the Doi and Edwards (DE) orientation tensor assuming an independent alignment (IA) of tube segments [8], which is five times the second order orientation tensor $\mathbf{S}$,

$$\mathbf{S}_{\mathrm{DE}}^{\mathrm{IA}}(t,t') \equiv 5\left\langle \frac{\mathbf{u}'\mathbf{u}'}{u'^2} \right\rangle = 5\mathbf{S}(t,t') \qquad (2)$$

u' presents the length of the deformed unit vector $\mathbf{u}'$, and the bracket denotes an average over an isotropic distribution of unit

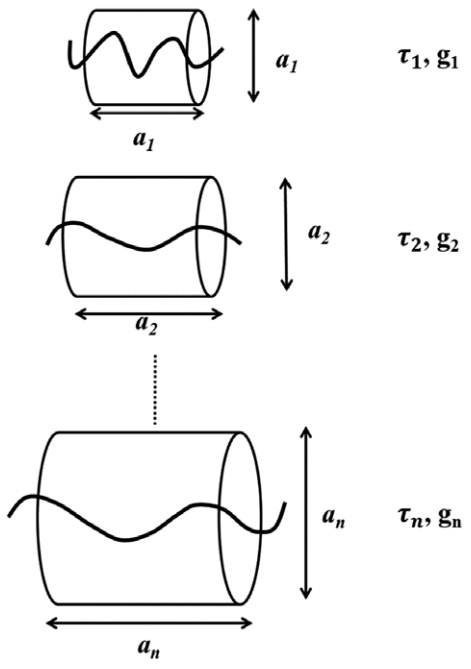

FIG. 2. Subdivision of an ensemble of polydisperse linear polymer chains into a series of hierarchically increasing tube diameter segments, characterized by increasing relaxation times; that is, $a_1 < a_2 < \cdots < a_n$ and $\tau_1 < \tau_2 < \cdots < \tau_n$. For details see text. Reprinted from [4], Copyright (2016), with permission from Elsevier.

DOI 10.1002/pen

vectors at time t', $\mathbf{u}(t')$, which can be expressed as a surface integral over the unit sphere,

$$\langle\rangle \equiv \frac{1}{4\pi}\oiint [\,]\sin\theta_0 d\theta_0 d\varphi_0 \tag{3}$$

The relative deformation gradient tensor, $\mathbf{F}^{-1}(t, t')$, signifies the deformation of the unit vector $\mathbf{u}$ at observation time t to $\mathbf{u}'$ according to affine deformation assumption,

$$\mathbf{u}'(t,t') = \mathbf{F}^{-1}(t,t').\mathbf{u}(t') \tag{4}$$

The molecular stress functions $f_i = f_i(t, t')$ are the inverse of the relative tube diameters a_i of each mode i,

$$f_i(t,t') = a_{i0}/a_i(t,t') \tag{5}$$

$f_i = f_i(t, t')$ is a function of both the observation time t and the time t' of creation of tube segments by reptation. The relaxation modulus $G(t)$ of the melt is represented by discrete Maxwell modes with partial relaxation moduli g_i and relaxation times τ_i,

$$G(t) = \sum_{j=1}^{n} G_i(t) = \sum_{j=1}^{n} g_j \exp(-t/\tau_j) \tag{6}$$

Please note that the hierarchical relaxation and dilution of the tube segments according to Figs. 1 and 2 are included in the linear-viscoelastic relaxation spectrum, and can therefore be extracted from the spectrum, as shown in the following.

In contrast to the case of *monodisperse* and *bidisperse* polymer melts, where dynamic dilution starts from the plateau modulus G_N^0 [3], there exist two dilution regimes during the relaxation process of *polydisperse* polymers: the regime of permanent dilution, and the regime of dynamic dilution. Permanent dilution occurs due to the presence of oligomeric chains and un-entangled (fluctuating) chain ends. As shown in Fig. 3, we assume that the onset of dynamic dilution occurs only when the relaxation process has reached the dilution modulus $G_D \le G_N^0$. The dilution modulus G_D is a free parameter of the model, which needs to be fitted to nonlinear viscoelastic experimental evidence, since the mass fraction of oligomeric chains and un-entangled chain ends is not known a-priori. The time when $G(t)$ has relaxed to the value of G_D, that is, $t = \tau_D$, denotes the commencement of the dynamic dilution zone, while at relaxation times $t \le \tau_D$, the chain segments are assumed to be permanently diluted. Hence, the relaxation time $t = \tau_D$ separates the zone of permanent dilution from the zone of dynamic dilution.

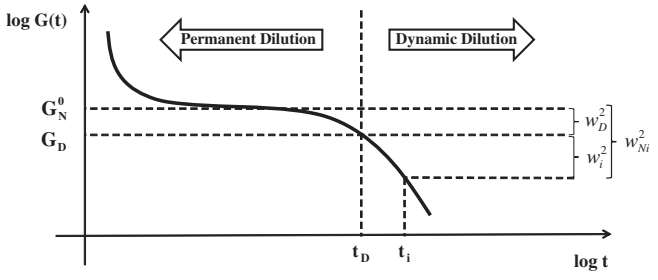

FIG. 3. Relaxation modulus and dilution dependent weight fractions of a chain segment with relaxation time τ_i in view of the permanent and dynamic dilution mechanisms of the HMMSF model. Reprinted with permission from [3]. Copyright [2016], The Society of Rheology.

The mass fraction w_i of dynamically diluted linear or LCB polymer segments with relaxation time $\tau_i > \tau_D$ is determined by considering the ratio of the relaxation modulus at time $t = \tau_i$ to the dilution modulus $G_D = G(t = \tau_D)$,

$$\begin{aligned} w_i^2 &= \frac{G(t=\tau_i)}{G_D} = \frac{1}{G_D}\sum_{j=1}^{n} g_j \exp(-\tau_i/\tau_j) \quad \text{for } \tau_i > \tau_D \\ w_i^2 &= 1 \qquad\qquad\qquad\qquad\quad \text{for } \tau_i \le \tau_D \end{aligned} \tag{7}$$

It is assumed that the value of w_i obtained at $t = \tau_i$ can be attributed to the chain segments with relaxation time τ_i. Segments with $\tau_i < \tau_D$ are considered to be permanently diluted that is, their weight fractions are fixed at $w_i = 1$. Although this may seem to be a very rough estimate, it was shown to be a sufficiently robust assumption to model the rheology of broadly distributed polymers, largely independent of the number of discrete Maxwell modes used to represent the relaxation modulus $G(t)$ [1].

The evolution equation for the molecular stress function of each mode is expressed as [1],

$$\frac{\partial f_i}{\partial t} = f_i(\mathbf{K}:\mathbf{S}) - \frac{f_i - 1}{\tau_{Ri}}\left(1 - \frac{2}{3}w_i^2\right) - \frac{2f_i^2(f_i^3 - 1)}{3\tau_{Ri}}w_i^2 \tag{8}$$

with the initial conditions $f_i(t = t', t) = 1$. The first term on the right hand side represents an on average affine stretch rate with $\mathbf{K}$ the velocity gradient tensor, the second term takes into account Rouse relaxation in the longitudinal direction of the tube, and the third term limits molecular stretch due to the interchain tube pressure in the lateral direction of a tube segment [9]. The effect of dynamic dilution is entering *Eq.* 8 via w_i^2, and takes into account that the effect of dynamic dilution vanishes in fast flows as discussed [1]. τ_{Ri} are the Rouse stretch-relaxation times of each mode, and the relation between τ_{Ri} and relaxation times τ_i as discussed in detail in [3,4] is summarized below.

Linear polymer melts. For linear polymer melts, we derived the relation

$$\tau_{Ri} = \frac{1}{3\kappa^{1.4}}\tau_i \tag{9}$$

where the parameter κ depends on the polydispersity of the system. In the case of well-entangled monodisperse linear polymers (i.e., when the dilution modulus is equal to the plateau modulus G_N^0), excellent agreement between the predictions of the HMMSF model with elongational viscosity data of monodisperse polystyrene melts was found for a value of κ=9, while κ reduces to κ=2 for a bidisperse blend of two monodisperse polystyrenes. For polydisperse linear melts, the value of κ is equal to 1, thus, the relation between Rouse stretch-relaxation times and relaxation times of **polydisperse linear polymers** is given by,

$$\tau_{Ri} = \tau_i/3 \tag{10a}$$

It is well known that star-shaped polymers featuring only one branch point per molecule show similar rheological behavior as linear polymers. We showed that *Eq. 10* a is also valid for polymers with predominantly star architecture such as sparsely branched metallocene catalysed polymers with typically less than one side branch per molecule [3].

LCB polymer melts. The situation regarding stretch relaxation of LCB polymers with more than one branch point is different: Although the stretch relaxation dynamics of linear polymers is governed by the Rouse time of the respective mode, the relaxation dynamics of a pom-pom polymer (restricted by two branch points in their stress relaxation) is governed by its relaxation time. Therefore, for LCB polymers, the stretch-relaxation times are equal to the relaxation times,

$$\tau_{Ri} = \tau_i \tag{10b}$$

Evolution equation for polydisperse linear and LCB melts. From *Eqs. 8-10*, a unified formulation of the evolution equations of the HMMSF model is given by

$$\frac{\partial f_i}{\partial t} = f_i(\mathbf{K}:\mathbf{S}) - \frac{f_i - 1}{\alpha\tau_i}\left(1 - \frac{2}{3}w_i^2\right) - \frac{2f_i^2\left(f_i^3 - 1\right)}{3}w_i^2 \tag{11}$$

The topological parameter α depends on the topology of the melt, with

$$\begin{aligned} &\alpha = 1 \text{ for LCB Melts} \\ &\alpha = 1/3 \text{ for polydisperse linear melts} \end{aligned} \tag{12}$$

Thus, the HMMSF model for polydisperse polymer melts consists of the multi-mode stress equation, *Eq. 1*, a set of evolution equations for the molecular stresses f_i, *Eq. 11*, and a hierarchical procedure to quantify the fraction of dynamically diluted chain segments according to *Eq. 7* with only one free nonlinear parameter, the dilution modulus G_D. Although the dilution modulus G_D for well-entangled mono- and bidisperse melts is equal to the plateau modulus G_N^0 [3], it is not known a-priory for polydisperse polymer melts which contain unknown fractions of non-entangled or marginally entangled oligomeric chains and chain ends. Once the linear-viscoelastic relaxation spectrum of a polydisperse polymer melt is known, the weight fractions w_i in the evolution *Eq. 11* can be obtained by fitting the value of G_D to the elongation viscosity. The parameter G_D, in conjunction with the relaxation times τ_i, determines the extent of strain hardening. This one free parameter is sufficient for modelling extensional flows, while in addition for shear flows, as explained in the following, a CR parameter is needed.

Shear Flows. We showed in [5] that the lack of satisfactory agreement between the HMMSF model and shear deformation data for an LCB melt is due to the absence of a flow dependent phenomenon termed the convective constraint release (CCR) relaxation mechanism. In this section, we summarize the incorporation of CCR into the HMMSF model.

The occurrence of CCR was originally introduced in the tube model by Marrucci [10] and Ianniruberto and Marrucci [11]. The CCR mechanism explains that when the shear rate is significantly greater than the inverse of the longest relaxation time, topological constraints are removed due to convection caused by the flow. Ianniruberto and Marrucci [11] stated that the chains under flow exhibit an inward motion relative to their tubes, and consequently this inward motion brings about the retraction of the chains within their tubes leading to the removal of the topological constraints for other chains. Therefore, reptation and the CCR relaxation mechanism collaborate in the relaxation of the entanglements at high strain rates in polydisperse systems. Ianniruberto and Marrucci assumed that combined impact of reptation and CCR on the overall relaxation frequency $1/\tau$ can be expressed as [11],

$$\frac{1}{\tau} = \frac{1}{\tau_0} + \beta\mathbf{K}:\mathrm{S} \tag{13}$$

Here $\frac{1}{\tau_0}$ is the reptation renewal frequency that is, the inverse of the reptation time τ_0, $\beta\mathbf{K}:\mathbf{S}$ the CCR renewal frequency, and β is the numerical coefficient of the CCR mechanism considered as a fitting parameter. Recently, Ianniruberto [12] generalized this idea to the polydisperse case, and formulated CCR for a multi-mode model.

We follow these ideas insofar, as we replace the linear-viscoelastic relaxation times τ_i in the evolution *Eq. 11* of the molecular stress function by CR relaxation times $\tau_{i\mathrm{CR}}$ defined as [5],

$$\frac{1}{\tau_{i\mathrm{CR}}} = \frac{1}{\tau_i} + \beta\ \mathrm{CR} \tag{14}$$

CR represents a dissipative CR term. In the formulation of CR we follow Wagner et al. [13], and express CR as,

$$\mathrm{CR} = \sqrt{|\mathbf{W}\cdot\mathbf{D}:\mathbf{S}|} \tag{15}$$

with

$$\begin{aligned} \mathbf{D} &= \frac{1}{2}\left(\mathbf{K} + \mathbf{K}^T\right) \\ \mathbf{W} &= \frac{1}{2}\left(\mathbf{K} - \mathbf{K}^T\right) \end{aligned} \tag{16}$$

D is the rate of deformation tensor, and **W** the rate of rotation tensor.

Alternatively, for steady shear flows, *Eq. 15* can be expressed in terms of the second order Rivlin-Ericksen tensors $\mathbf{A}_1$ and $\mathbf{A}_2$,

$$\begin{aligned} \mathbf{A}_1^2 &= 4\mathbf{D}^2 \\ \mathbf{A}_2 &= \mathbf{A}_1^2 + 2\left(\mathbf{W}\cdot\mathbf{D} + \mathbf{D}\cdot\mathbf{W}^T\right) \end{aligned} \tag{17}$$

resulting in

$$\mathrm{CR} = \frac{1}{2}\sqrt{\left|\mathbf{A_2}:\mathbf{S}\text{-}\mathbf{A_1^2}:\mathbf{S}\right|} \tag{18}$$

It is obvious from *Eqs 15* and *17* that CR is identical to zero in irrotational (extensional) flows, while in simple shear flows, CR is given by

 DOI 10.1002/pen

$$\mathrm{CR}=\frac{1}{2}\sqrt{\dot{\gamma}^2|S_{11}-S_{22}|} \tag{19}$$

As schematically depicted in Fig. 4, the different effect of CR in extensional vs. shear flow can be explained in the following way: During extensional deformation, any CR effect is compensated by the advection of the neighbouring topological constraints in the direction of flow (Fig. 4a). This results in a minimum of the tube diameter and a maximum molecular stress function, $f_{\max}$ [13,14], under steady-state conditions. On the other hand in shear flow, when the tube segment is aligned in the flow direction at high shear strains (Fig. 4b), the topological constraints above and below the chain are released, and the tube diameter tends to return to its equilibrium value a_0. Therefore, while CR has no effect in extensional flows, it is indispensable to incorporate a dissipative CR mechanism at higher shear strains into the HMMSF model.

Introducing convective CR, the evolution equation of the HMMSF model for polydisperse linear and LCB melts in extensional as well as shear flows, *Eq. 11*, becomes,

$$\frac{\partial f_i}{\partial t}=f_i(\mathbf{K}:\mathbf{S})-\frac{f_i-1}{\alpha\tau_{iCR}}\left(1-\frac{2}{3}w_i^2\right)-\frac{2f_i^2\left(f_i^3-1\right)}{3}\frac{}{3\alpha\tau_{iCR}}w_i^2 \tag{20}$$

with τ_{iCR} from *Eq. 14*, or

$$\frac{\partial f_i}{\partial t}=f_i(\mathbf{K}:\mathbf{S})-\frac{1}{\alpha}\left(\frac{1}{\tau_i}+\beta CR\right)\left[(f_i-1)\left(1-\frac{2}{3}w_i^2\right)+\frac{2}{9}f_i^2\left(f_i^3-1\right)w_i^2\right] \tag{21}$$

The HMMSF model with the stress tensor given by *Eq. 1*, the evolution *Eq. 21* for polydisperse linear (α = 1/3) and LCB (α = 1) polymer melts, and the diluted mass fractions w_i according to *Eq. 7* can now be used to predict the overall rheological behaviors in both extensional and shear flows with only two nonlinear parameters that is, G_D (dilution modulus) and β (CR parameter). For extensional flows with CR = *0*, only one nonlinear parameter is needed, the dilution modulus G_D.

EXPERIMENTAL

Materials

To demonstrate the versatility and accuracy of the HMMSF model, we present in the following a comparison of model predictions and experimental data for a variety of linear and LCB polymers spanning the full regime of commercial polyolefins. We consider a well characterized low-density polyethylene (LDPE I) melt tested in elongation, biaxial and planar extension, as well as shear flow [13, 15–18]); a tubular (LDPE III) and an autoclave LDPE (LDPE V) tested in elongation [15]; a well characterized high-density polyethylene (HDPE I) melt tested in elongation, biaxial and planar extension, as well as shear flow ([15,16]); a proprietary grade of metallocene catalyzed polyethylene (mPE 4); and a linear LDPE (LLDPE) tested in elongation [15,16].

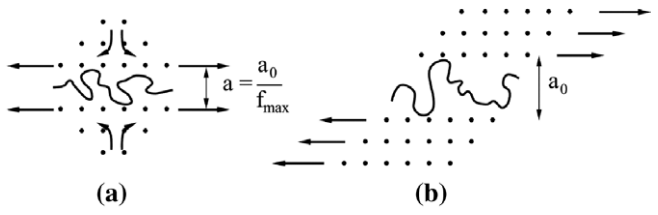

FIG. 4. (a) In extensional flow and large strains, any CR effects are compensated by the advection of neighboring topological constraints, leading to a minimum tube diameter a and a maximum molecular stress $f_{\max}$. (b) In shear flow and large strains, the molecule is simply oriented in the flow direction and, due to convective CR above and below the molecular chain, the tube diameter returns to its equilibrium value a_0. Adapted from [15].

Tables 1 and 2 display the architecture, and as far as available, weight average molecular weight (M_w), number average molecular weight (M_n), polydispersity index (M_w/M_n), melting temperature (T_m), testing temperature (T), room temperature density (ρ_{RT}), testing temperature density (ρ_T), zero shear viscosity at testing temperature (η_0), melt flow index (MFI), activation energy (E_a), dilution modulus G_D (as obtained by fitting of the elongational data), the constrain release parameter β, and the linear-viscoelastic relaxation spectrum of the polymers at the testing temperatures.

Rheological Measurments

The elongational rheological measurements were conducted by a commercial form of the Meissner rheometer manufactured by Rheometric Scientific, and named Rheometrics Melt Extensional Rheometer (RME) [15]. The comprehensive aspects of this commercial rheometer, as well as the rheological theories behind it have has been explained elsewhere [19,20]. The equibiaxial and planar elongational measurements were performed by new directional arrangements of the metal belts of the RME clamps that is, in a circle for equibiaxial tests and in a rectangle for planar tests. The details of the modified version of the biaxial extensional rheometer are described in [17]. The steady shear rheological measurements of LDPE I were conducted by Kraft [18] and Bastian [13,15] through cone-and-plate configuration (0.1 rad gap angle) in strain-controlled rheometers (RMS 800, Rheometric Scientific™) at 150°C (LDPE I) and 170°C (HDPE I). The significance of these data is due to their separate measurements and reproducibility in different laboratories that is, the Polymer Physics Lab at ETH Zurich, Switzerland, and the IKT at Stuttgart, Germany. In the figures, the measurements at the ETH [18] are denoted by "Kraft", while the measurements of Bastian. [13] are denoted by "IKT". We think that the differences seen between the two datasets at the higher shear rates are an honest account of the achievable measurement accuracy.

COMPARISON BETWEEN HMMSF MODEL PREDICTIONS WITH EXPERIMENTAL DATA IN EXTENSION AND SHEAR

LCB Polymer Melts

Figure 5 compares the multiaxial extensional viscosity data of LDPE I (Lupolen 1810H) [16] with the predictions of the HMMSF model for LCB melts in extensional flows (*Eqs. 1*, *7*, *11*, and *12*). The symbols in Fig. 5 present the uniaxial, equibiaxial, and planar transient viscosities of LDPE I at 150°C, and predictions of the HMMSF model are illustrated by continuous lines. The HMMSF model shows a very good agreement with the uniaxial extensional viscosity of LDPE I during the strain hardening regime and its transition to the steady-state extensional viscosity (Fig. 5). The slight under-prediction of the uniaxial extensional viscosity, η_E^+, at the two lowest elongation rates of $\dot{\varepsilon}=0.003\,\text{and}\,0.0102\,s^{-1}$ is due the limited extension of the relaxation

TABLE 1. Characterization and relaxation spectrum of LDPE I, LDPE III, and LDPE V

Characteristics	LDPE I		LDPE III		LDPE V	
Product	Lupolen 1810H		Tubular		Autoclave	
Producer	BASF		-		-	
Architecture	LCB		LCB		LCB	
M_w [g/mol]	188,000		119,000		130,000	
M_n [g/mol]	16,600		24,600		21,900	
M_w/M_n	11.3		4.85		5.95	
T_m [°C]	110		-		-	
T [°C]	150		150		150	
ρ_{RT} [g/cm^3]	0.917		0.923		0.921	
ρ_T [g/cm^3]	0.778		0.78		0.78	
η_0 (@ T) [kPa.s]	72.5		75.2		55.2	
MFI [g/10 min]	1.2		-		-	
E_a [kJ/mol]	58.6		62.8		57.2	
G_D [Pa]	1.50E + 04		1.00E + 04		4.00E + 04	
β [−]	0.14		-		-	
Rheometer	Meissner-type and RMS 800		RME (IKT)		RME (IKT)	
Relaxation Spectrum at T						
I	g_i [Pa]	τ_i [s]	g_i [Pa]	τ_i [s]	g_i [Pa]	τ_i [s]
1	3.00E-01	5.00E + 03	9.19E + 05	1.20E-04	1.53E + 05	2.06E-03
2	4.59E + 00	1.00E + 03	7.28E + 04	5.64E-03	5.65E + 04	1.73E-02
3	2.75E + 02	1.00E + 02	3.33E + 04	2.94E-02	3.01E + 04	1.06E-01
4	2.58E + 03	1.00E + 01	2.19E + 04	1.38E-01	1.37E + 04	6.18E-01
5	9.80E + 03	1.00E + 00	1.10E + 04	7.00E-01	4.65E + 03	3.44E + 00
6	2.97E + 04	1.00E-01	4.54E + 03	3.52E + 00	9.68E + 02	1.92E + 01
7	5.20E + 04	1.00E-02	1.36E + 03	1.71E + 01	5.85E + 01	1.31E + 02
8	-	-	2.33E + 02	8.25E + 01	-	-
9	-	-	4.90E + 00	8.99E + 02	-	-

spectrum of LDPE I, and consequently the underestimation of the weight of the longest relaxation time, which leads to an inaccurate prediction of the elongational viscosity of the polymer at low strain rates. Figure 5b shows that the predictions of the HMMSF model are in excellent quantitative agreement with the equibiaxial viscosity of LDPE I, η_B^+. Moreover, the HMMSF model presents

TABLE 2. Characterization and relaxation spectrum of HDPE I, mPE 4, and LLDPE

Characteristics	HDPE I		mPE 4		LLDPE	
Product	HDPE		Metallocene-catalyzed Polyethylene		Affinity PL 1880	
Producer	Statoil/Norway		-		Dow	
Architecture	Linear		Linear and Star		Linear	
M_w [g/mol]	104,000		-		116,400	
M_n [g/mol]	18,900		-		55,100	
M_w/M_n	5.5		-		2.1	
T_m [°C]	138		-		102.5	
T [°C]	150 (extension), 170 (shear)		150		130	
ρ_{RT} [g/cm^3]	0.951		0.923		0.918	
ρ_T [g/cm^3]	0.778		-		0.757	
η_0 (@ T) [kPa.s]	127.4 (150 °C)		98.1		93.8	
MFI [g/10 min]	-		-		-	
E_a [kJ/mol]	27		-		41.5	
G_D [Pa]	8.00E + 2		3.00E + 04		9.00E + 02	
β [−]	1		-		-	
Rheometer	Meissner-type and RMS 800		RME		RME	
Relaxation Spectrum at T						
I	g_i [Pa]	τ_i [s] (150, 170 °C)	g_i [Pa]	τ_i [s]	g_i [Pa]	τ_i [s]
1	1.54E + 05	1.41E-02, 1.00E-02	2.36E + 05	2.66E-03	4.83E + 05	1.00E-03
2	3.19E + 04	1.41E-01, 1.00E-01	4.49E + 04	2.00E-02	2.80E + 05	7.20E-03
3	7.82E + 03	1.41E + 00, 1.00E + 00	1.97E + 04	1.02E-01	1.27E + 05	5.18E-02
4	1.41E + 03	1.41E + 01, 1.00E + 01	8.64E + 03	4.87E-01	2.97E + 04	3.73E-01
5	1.99E + 02	1.41E + 02, 1.00E + 02	3.98E + 03	2.06E + 00	6.97E + 03	2.68E + 00
6	2.07E + 01	1.41E + 03, 1.00E + 03	1.84E + 03	7.67E + 00	1.79E + 03	1.93E + 01
7	4.58E + 00	7.07E + 03, 5.00E + 03	8.53E + 02	2.73E + 01	1.36E + 02	1.39E + 02
8	-	-	3.65E + 02	1.23E + 02	1.46E + 00	1.00E + 03

DOI 10.1002/pen

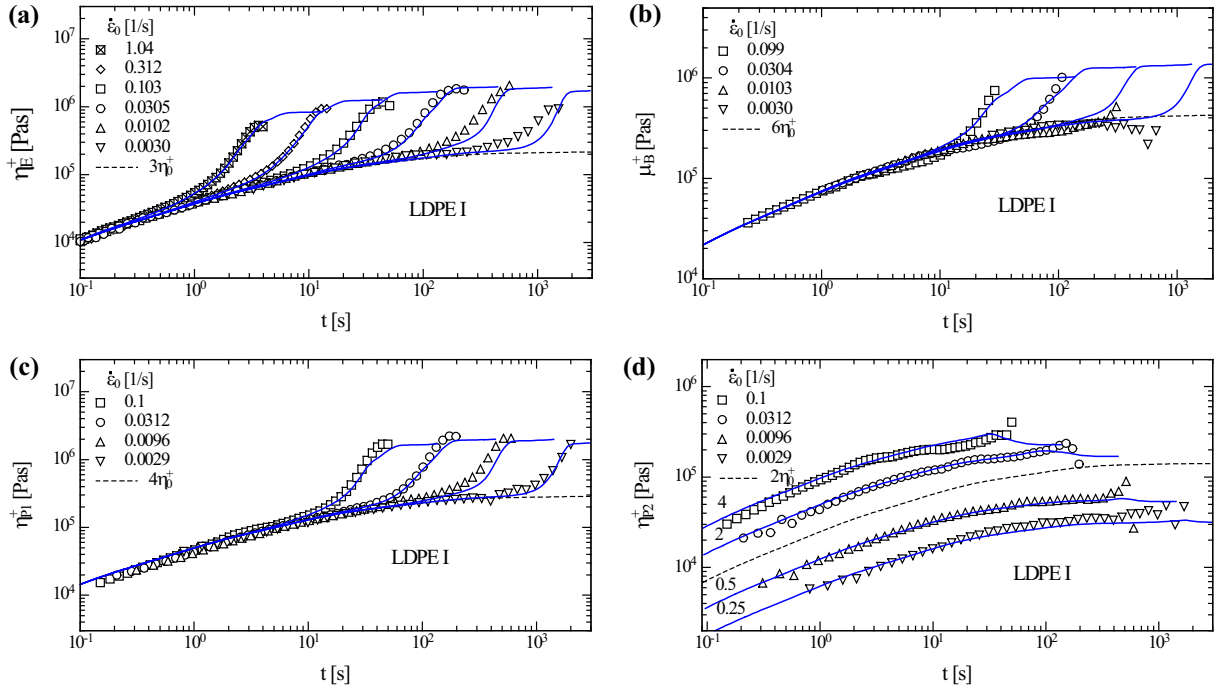

FIG. 5. Comparison of (a) uniaxial, (b) equibiaxial, as well as (c and d) first and second planar viscosity data (symbols) of LDPE I (Lupolen 1810H) melt at 150°C with predictions of the HMMSF model (*Eqs. 1, 7, 11*, and *12*, continuous lines) for a dilution modulus of G_D = *1.5E + 4 Pa.* Dotted line indicates the linear-viscoelastic start-up viscosities. Data and lines in (d) are shifted by factors 4, 2, 0.5, and 0.25 vertically. Reprinted by permission from Springer [2], Copyright (2016). [Color figure can be viewed at wileyonlinelibrary.com]

a remarkably accurate prediction of the planar extensional viscosity of LDPE I in the direction of flow, also called first planar viscosity (η_{P1}^+), in both qualitative and quantitative scales (Fig. 5c). η_{P1}^+ exhibits noteworthy similarities with its uniaxial counterpart as was already noticed by Hachmann and Meissner [17]. In contrast to η_{P1}^+, the second planar viscosity η_{P2}^+, also called cross viscosity, does not display strain hardening behaviour, and in fact, Hachmann and Meissner stated that the cross viscosity of LDPE I always shows undershoots ($\eta_{P2}^+/2\eta_0^+ < 1$) except for the smallest Hencky rates (Fig. 5d). The predictions of the HMMSF model are also in good agreement with the cross viscosity of the planar extensional mode. We may add that the existence of small maxima in the η_{P2}^+ data can be inferred from the experiments at strain rates 0.0312 and 0.0096 *1/s.* These maxima, which are predicted by the HMMSF model, are due to the strain dependence of the difference $S_{22} - S_{33}$ of the orientation tensor components S_{22} and S_{33}, and are already predicted by the DE IA model [21]. Only the intensity and location of the maxima in the time or strain domain are affected by the isotropic stretch.

Also in the case of the other two LCB melts considered here, the predictions of the elongational viscosity of LDPE III and V (continuous lines in Fig. 6) are in excellent agreement with the experimental data for the time-dependent strain-hardening regime, and as far as accessible by the experiments, in the transition to what seems to be a steady-state elongational viscosity. It is obvious that the experimental data do not allow inferring a definite steady-state elongational viscosity at all strain rates, and thus the prediction represents rather a lower limit of the steady-state value. We also note that the HMMSF model does not accommodate for the branch point withdrawal mechanism [22] which may be

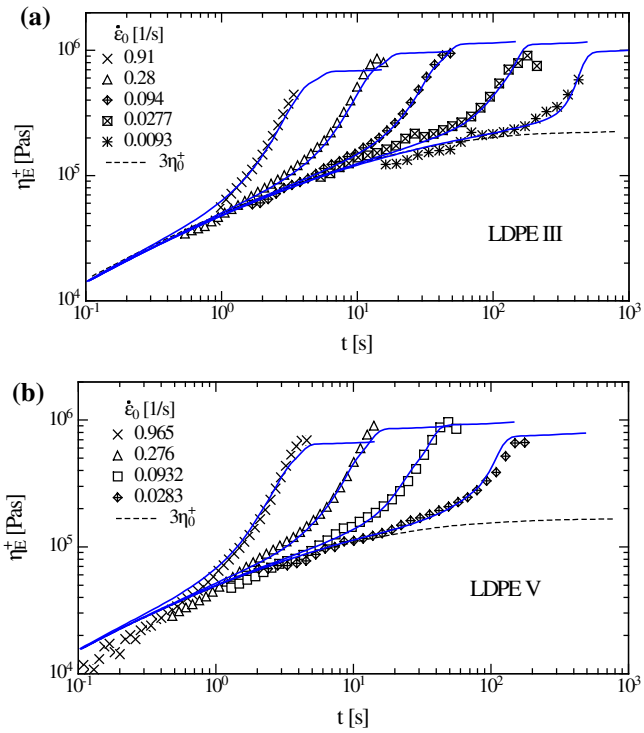

FIG. 6. Comparison of elongational viscosity data (symbols) of LDPE III and LDPE V at 150 °C measured by RME rheometer [15], with predictions of HMMSF model (*Eqs. 1, 7, 11*, and *12*); continuous lines) with G_D = 1.0E + 04, and 4.0E + 04 Pa, respectively. Reprinted by permission from Springer [1], Copyright (2016). [Color figure can be viewed at wileyonlinelibrary.com]

significant in modelling of the maxima of the viscosity in uniaxial extensional flow as observed by Bach et al. [23], Rasmussen et al. [24], and Alvarez et al. [25] for several (but not all) LDPEs. Instead, the HMMS model assumes that the stretch of the backbone segments is balanced by the interchain pressure, which leads to a prediction of a steady-state extensional viscosity without a maximum. The slight under-prediction observed at the lowest elongation rate in Fig. 6b is again due to the limited extension of the relaxation spectrum of the LDPE sample, and consequently the underestimation of the weight of the longest relaxation time.

Figure 7 shows the predictions of the start-up shear viscosity and the first normal stress function of LDPE I melt by the HMMSF model (*Eqs. 1*, *7*, *21*, and *12*). A dilution modulus of G_D = *1.5E + 4 Pa* and a CR parameter of β = *0.14* lead to good agreement of predictions with the shear data for both low and high shear rate deformations. The prediction of the maxima of the first normal stress function are in good accordance with the observed maxima (Fig. 7b). At high shear rates, the experimental signal is delayed due to rise-time effects caused by the limited stiffness of the rheometer leading to radial inflow of the melt (see e.g., [5] for more details).

Linear Polymer Melts

The HMMSF model for polydisperse linear polymer melts consists of the multi-mode stress equation (*Eq. 1*), a set of evolution equations for the molecular stresses f_i (*Eq. 11* with α = 1/3), and a hierarchical procedure to evaluate the effect of dynamic dilution (*Eq. 7*) with only one free non-linear parameter, the dilution modulus G_D. Once the linear-viscoelastic relaxation spectrum of a

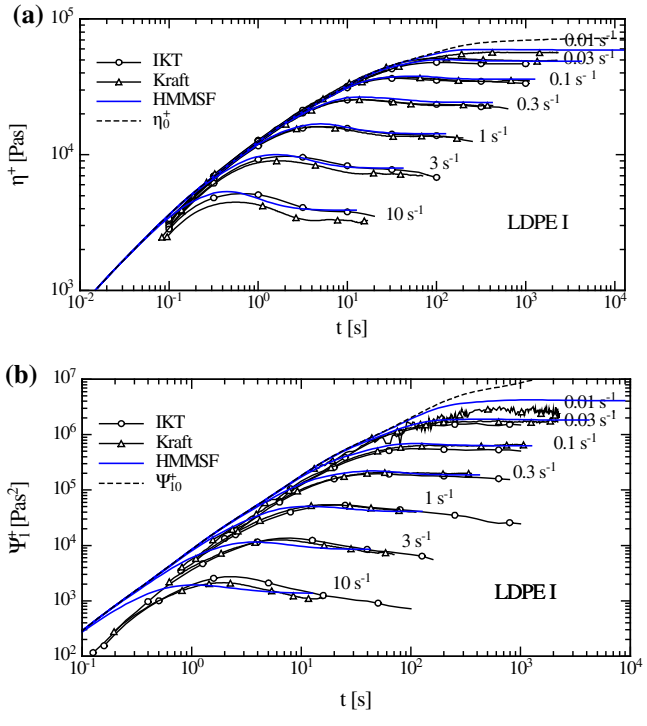

FIG. 7. Comparison of the predictions (blue lines) of the HMMSF model including the CR term (*Eqs. 1, 7, 21*, and *12* with G_D = *1.5E + 4 Pa* and β = *0.14* for LDPE I with (a) shear viscosity and (b) first normal stress function data (lines with symbols). Data by Kraft [18] and Bastian [13,15] (IKT)] at 150 °C. Reprinted by permission from Springer [5], Copyright (2016). [Color figure can be viewed at wileyonlinelibrary.com]

polydisperse linear polymer melt is known, the weight fractions w_i (due to dynamic dilution, which enter the evolution *Eq. 11* explicitly) can be obtained by fitting the value of G_D to the experimental evidence. The parameter G_D, in conjunction with the Rouse times $\tau_{Ri} = \tau_i/3$, determines the extent of strain hardening. The symbols in Fig. 8 present the uniaxial, equibiaxial, and planar transient viscosities (η_E^+, η_B^+, η_{P1}^+, and η_{P2}^+, respectively) of HDPE I at 150°C, and the predictions of the HMMSF model are illustrated by the use of continuous lines in the figures. The onset of strain hardening in HDPE I is attributed to the existence of very long chains in the molecular weight distribution leading to long relaxation times [17]. In the case of equibiaxial extensional deformation (Fig. 8b), η_B^+ of HDPE I demonstrated at first a viscosity lower than the linear-viscoelastic start-up viscosity, and then a limited strain hardening effect after the crossover point ($\eta_B^+ = 6\eta_0$). The viscosity of the planar extensional viscosity of HDPE I in the direction of flow (η_{P1}^+) exhibited similar strain hardening behavior as its uniaxial counterpart η_E^+, while the polymer does not show strain hardening in the cross-direction of flow that is, $\eta_{P2}^+ < 2\eta_0$ (Fig. 8c and d). The HMMSF model with a dilution modulus of G_D = *8.0E + 2 Pa* demonstrates excellent agreement with the uniaxial extensional viscosity of HDPE I (Fig. 8a) in the strain hardening regime and, as far as accessible by the experiments, in the transition to what seems to be the steady-state elongational viscosity. Figure 8b shows that the predictions of the HMMSF model are also in very good agreement with the equibiaxial viscosity data of HDPE I. Moreover, the model presents a remarkably fine prediction of the planar extensional viscosities of HDPE I in the direction of flow as well as in the cross-flow direction (η_{P1}^+ and η_{P2}^+) in both qualitative and quantitative scales (Fig. 8c and d, respectively).

Figure 9 illustrates the predictions of the uniaxial extensional viscosity of metallocene-catalyzed polyethylene (mPE 4), which consist of a mixture of linear and sparsely LCB (star-shaped) macromolecules, through the HMMSF model for linear polymers (*Eqs. 1, 7, 11,* and *12*). The elongational viscosity of mPE 4 is well described by the HMMSF model. mPE 4 is sparsely LCB that is, contains a fraction of asymmetric star molecules. As expected, star molecules featuring only one branch point show a similar nonlinearity in extensional flow as linear polymers. On the other hand, due to the narrow molecular weight distribution of metallocene-catalyzed polymers, there is less dilution by oligomers and chain ends, and the dilution modulus G_D is larger, leading to enhanced strain hardening of mPE 4. In contrast, Torres et al. [26] expect that mPEs produced via solution polymerization show weak strain hardening at moderate Hencky strain rates (0.1–1 s^{-1}), as the presence of branch points in H molecules are not sufficient to increase their strain hardening behavior. Although it is possible to produce mPEs which mainly consist of linear and star molecules [27], it is more likely that the occurrence of further branching leads to treelike molecules which can delay the relaxation of backbones, and hence, promote strain hardening [26].

Figure 10 presents the modelling of the elongational viscosities η_E^+ data of LLDPE I (linear melt) through the HMMSF model. Bearing in mind that only a single material parameter, the dilution modulus G_D, is needed, the model shows an outstanding consistency with the experimental data for the prediction of the strain hardening and the transition to the steady-state viscosity region.

As in the case of LCBs, good agreement is found when shear viscosity and first normal stress function data of HDPE I are

DOI 10.1002/pen

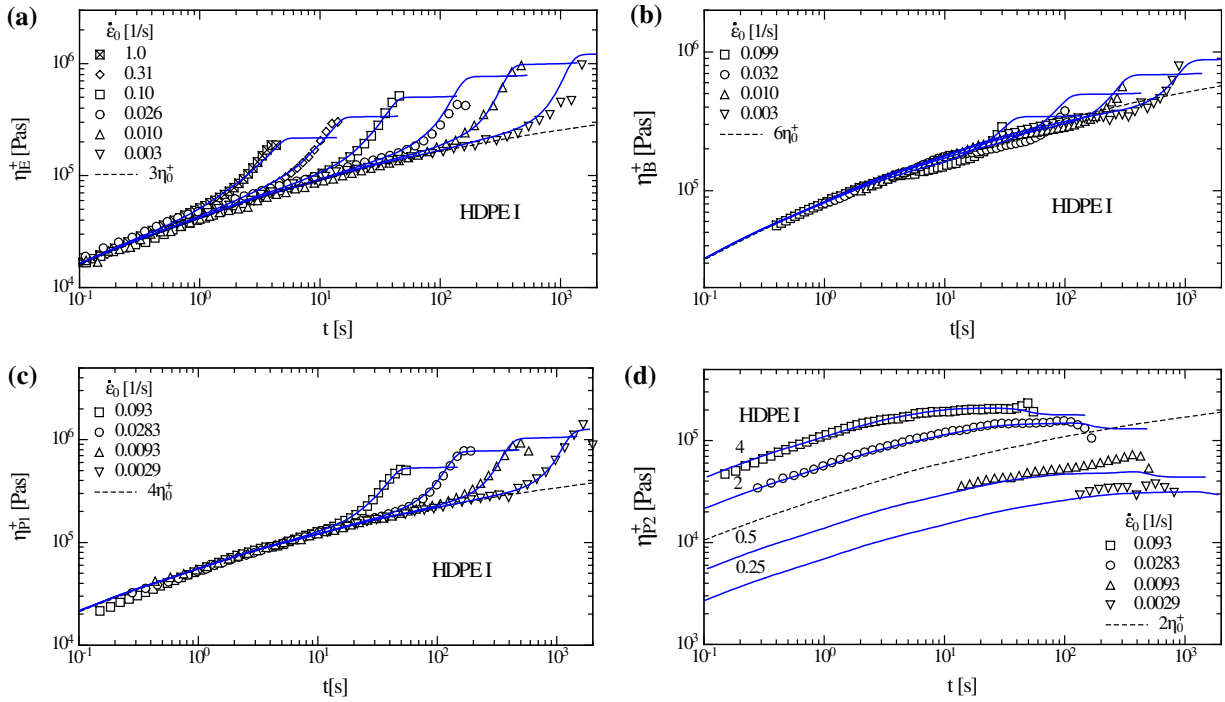

FIG. 8. Modelling of (a) uniaxial, (b) equibiaxial, (c) first planar, and (d) second planar extensional viscosity data (symbols) of HDPE I by the HMMSF model (*Eqs. 1, 7, 11*, and *12*; continuous lines) at 150°C with dilution modulus G_D = *8.0E + 2 Pa.* Data and lines in (d) are shifted by factors 4, 2, 0.5, and 0.25 vertically. Dotted lines indicate the linear-viscoelastic start-up viscosities. Reprinted with permission from [3]. Copyright [2016], The Society of Rheology. [Color figure can be viewed at wileyonlinelibrary.com]

compared with predictions of the HMMSF model for the shear flow of linear melts (*Eqs. 1, 7, 21,* and *12*) in Fig. 11a and b, respectively. The HMMSF model for linear melts with a dilution modulus of G_D = *1.5E + 4 Pa* and a CR parameter of β = *1* results in good prediction of the shear viscosity and first normal stress function at low and high shear rates. The main difference between the shear flow of LCB and linear melts is detected by the absence of the occurrence of maxima of the first normal stress function in linear melts at high shear rates (compare Figs. 7b vs. 11b).

It is worth mentioning that the DE tube model [28] offers good predictions for the shear behaviours of linear polymers. According to Wagner et al. [13], aside from some exceptions, the DE model demonstrates fair agreements with the experimental data of monodisperse linear entangled melts in the nonlinear viscoelastic range when the polymers undergo shear deformation. In the case of stress relaxation after step shear strains [29,30], the DE model shows excellent agreement with the experimental data of linear melts [31–33]. In terms of the HMMSF model, this can be understood by considering Fig. 4: in shear flows of linear melts, the effect of stretch nearly vanishes that is, $f_i(t, t') \cong 1$, and the HMMSF model reduces approximately to the DE model. The predictions of DE tube model (i.e., *Eq. 1* with $f_i(t, t') = 1$) for shear viscosity and first normal stress function of HDPE I are shown in Fig. 12a and b, respectively. The DE model predictions for shear

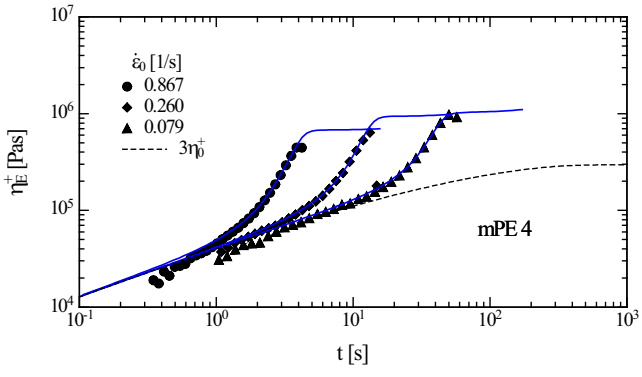

FIG. 9. Modeling of elongational viscosities of mPE 4 via the HMMSF model (*Eqs. 1, 7, 11*, and *12*) at 150°C with G_D = *3.0E + 04 Pa.* Dotted line indicates $3\eta_0^+(t)$. Reprinted from [4], Copyright (2016), with permission from Elsevier." [Color figure can be viewed at wileyonlinelibrary.com]

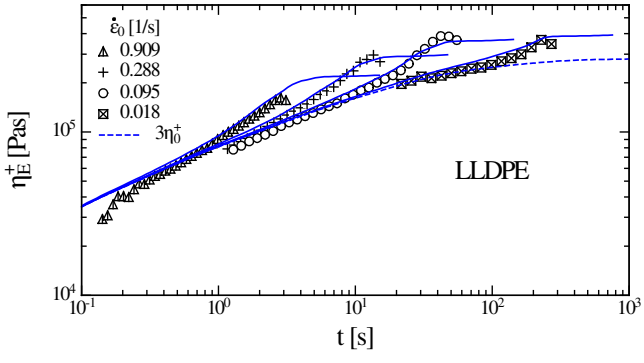

FIG. 10. Modeling of elongational viscosity data (symbols) of LLDPE with G_D = *9.0E + 2 Pa* by the HMMSF model (*Eqs. 1, 7, 11*, and *12*; continuous lines) at 130°C. Dotted line indicates $3\eta_0^+(t)$. Reprinted with permission from [3]. Copyright [2016], The Society of Rheology. [Color figure can be viewed at wileyonlinelibrary.com]

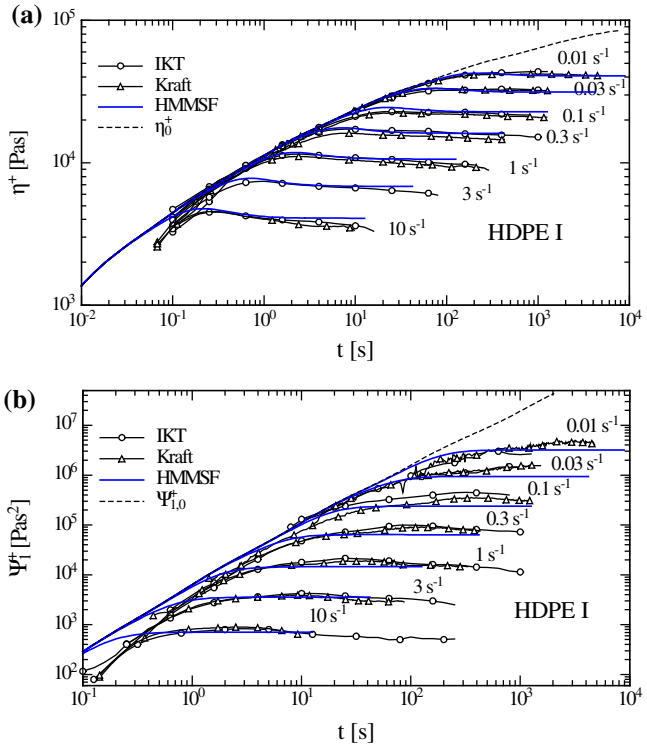

FIG. 11. Comparison of the predictions (full lines) of the HMMSF model including the CR term (*Eqs. 1, 7, 21*, and *12* with G_D = 800 Pa and β = *1*) with (a) shear viscosity and (b) first normal stress function data (lines with symbols) of HDPE I. Data of Kraft [18] and Bastian [13,15] (IKT) at 170°C. [Color figure can be viewed at wileyonlinelibrary.com]

viscosity are comparable to the predictions of the HMMSF model, while the DE model demonstrates a slight underprediction of the first normal stress function.

Application of the HMMSF Model in Predicting Crystallization Rate and Morphology of HDPE

In a recent study conducted by Hassager's group [34] on the effect of an ultra-high-molecular weight tail (UHMW-tail) on controlled uniaxial extension and the morphology of the quenched melt, they compared a blend of 1% UHMW polyethylene (UHMWPE; *M*w = 4,000 kg/mol) in a matrix of commercial HDPE with the pure matrix. The application of the HMMSF model on the uniaxial extension data of the UH-blend and the pure matrix at 140°C and strain rates of 0.03–1 s^{-1} with a dilution modulus of G_D = 350 Pa resulted in excellent prediction of the extensional rheological behavior of the samples. The model also revealed that the difference between the extensional behaviors of UH-blend and matrix is a result of the very large stretch of the highest modes leading to a squared contribution to stress. Further, they showed that the rate of shish nucleation, $\dot{N}_s$, is dependent on the relevant stretch ratio Λ at the onset of crystallization, $\dot{N}_s \propto \Lambda^4 - 1$. Accordingly, they calculated the average crystallization rate proportionality, $\langle \Lambda^4 - 1 \rangle$, from the stretch f_i of each mode in the HMMSF model and demonstrated that a very small fraction of UHMW component in a semicrystalline polymer melt has a significant impact on its extensional rheology as well as on the final morphology.

CONCLUSIONS

The general guideline in the development of the HMMSF model has been to recognize that the rheological effects of the complex molecular structures of polymers are already contained in the linear-viscoelastic relaxation modulus, and that only a limited number of well-defined constitutive assumptions concerning the nonlinear rheology is needed. The HMMSF model for LCB and linear polymer melts is established on four basic concepts: (1) hierarchal relaxation, (2) dynamic dilution, (3) interchain tube pressure, and (4) convective CR. Through hierarchical relaxation, dynamic dilution results in larger tube diameters of chain segments with longer relaxation times τ_i. The onset of dynamic dilution occurs when the relaxation process reaches the dilution modulus $G_D \le G_N^0$, and the "dynamic" part of dilution (as quantified by the dilution modulus G_D) vanishes gradually with increasing Weissenberg number $Wi_{Ri} = \dot{\varepsilon}\tau_{Ri}$ in the nonlinear viscoelastic regime. Stretch and orientation dynamics of the HMMSF model are coupled through a tube diameter which decreases with increasing deformations. A decreasing tube diameter in turn leads to an increasing interchain tube pressure, which sets a limit on the minimum tube segment diameter, and thereby the maximum stretch of the chain segment for a given deformation rate. The incorporation of a dissipative CR mechanism into the HMMSF model reduces chain stretch at larger shear deformations and shear rates, but has no effect in extension. The necessity of CR merely in the case of shear flows was implemented in the evolution equation of the molecular stress function by use of a specific combination of the second order Rivlin-Ericksen tensors

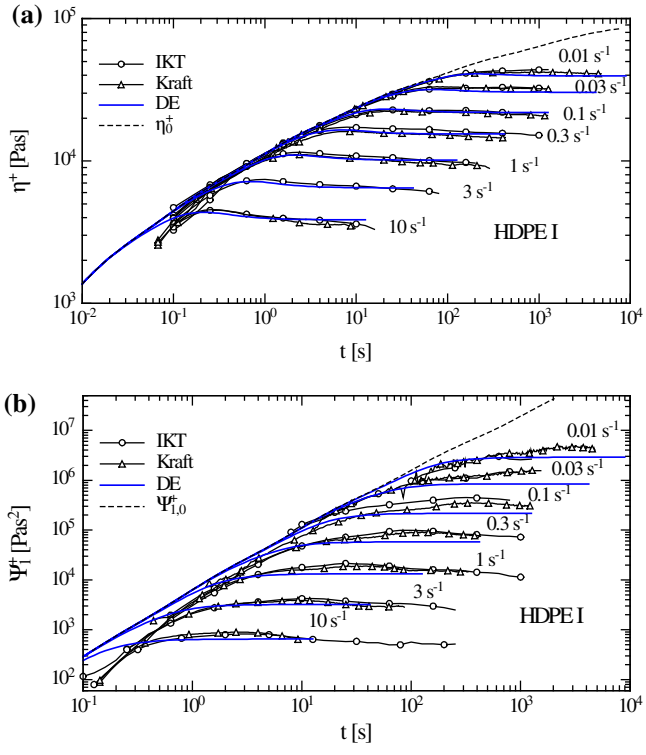

FIG. 12. Comparison of the predictions (full lines) of the DE model (i.e., *Eq. 1* with $f_i(t, t') = 1$) for linear melts with (a) shear viscosity and (b) first normal stress function data (lines with symbols) of an HDPE I. Data of Kraft [18] and Bastian [13,15] (IKT) at 170°C. [Color figure can be viewed at wileyonlinelibrary.com]

DOI 10.1002/pen

in such way that CR is only active in shear flows. The HMMSF model consists of an extremely simple set of equations:

(a) The multi-mode stress equation, *Eq. 1*.

(b) A hierarchical procedure to evaluate the effect of dynamic dilution, *Eq. 7*.

(c) A set of evolution equations for the molecular stress functions f_i, *Eq. 21*.

The HMMSF model, with only one nonlinear material parameters in uniaxial and multiaxial extensional flows, namely the dilution modulus G_D, and an additional CR parameter β in shear flow, is effectively capable of modeling the extensional and shear data of linear and LCB polymer melts at all extensional and shear rates investigated. Therefore, the HMMSF model with two nonlinear parameters is expected to successfully predict also all types of mixed flows (involving both shear and extensional deformations) which are significant to melt processing techniques. However, this remains to be proven by numerical simulations of mixed flows.

REFERENCES

1. E. Narimissa, V.H. Rolón-Garrido, and M.H. Wagner, *Rheol. Acta*, **54**, 9 (2015).
2. E. Narimissa, V.H. Rolón-Garrido, and M.H. Wagner, *Rheol. Acta*, **55**, 4 (2016).
3. E. Narimissa and M.H. Wagner, *J. Rheol.*, **60**, 4 (2016).
4. E. Narimissa and M.H. Wagner, *Polymer*, **104**, 204 (2016).
5. E. Narimissa and M.H. Wagner, *Rheol. Acta*, **55**, 8 (2016).
6. J.M. Dealy and R.G. Larson, Structure and Rheology of Molten Polymers - From Structure to Flow Behavior and Back Again, Hanser Publishers, Munich (2006).
7. E. Van Ruymbeke, H. Lee, T. Chang, A. Nikopoulou, N. Hadjichristidis, F. Snijkers, and D. Vlassopoulos, *Soft matter*, **10**(27), 4762 (2014).
8. M. Doi and S.F. Edwards, The Theory of Polymer Dynamics, Oxford University Press, Oxford (1986).
9. M.H. Wagner, S. Kheirandish, and O. Hassager, *J. Rheol.*, **49**, 6 (2005).
10. G. Marrucci, *J. Non-Newtonian Fluid Mech.*, **62**(2), 279 (1996).
11. G. Ianniruberto and G. Marrucci, *J. Non-Newtonian Fluid Mech.*, **65**, 2 (1996).
12. G. Ianniruberto, *J. Rheol.*, **59**, 1 (2015).
13. M.H. Wagner, P. Rubio, and H. Bastian, *J. Rheol.*, **45**, 6 (2001).
14. M.H. Wagner, H. Bastian, P. Hachmann, J. Meissner, S. Kurzbeck, H. Münstedt, and F. Langouche, *Rheol. Acta*, **39**(2), 97 (2000).
15. H. Bastian, Non-linear viscoelasticity of linear and long-chain-branched polymer melts in shear and extensional flows, 2001, Universität Stuttgart, Stuttgart, https://doi.org/10.18419/opus-1538.
16. P. Hachmann, Multiaxiale Dehnung von Polymerschmelzen, ETH Zurich, Zurich (1996). https://doi.org/10.3929/ethz-a-001732525.
17. P. Hachmann and J. Meissner, *J. Rheol.*, **47**, 4 (2003).
18. M. Kraft, Untersuchungen zur scherinduzierten rheologischen Anisotropie von verschiedenen Polyethylen-Schmelzen, *Diss. Techn. Wiss. ETH Zürich*, (1996).
19. J. Meissner and J. Hostettler, *Rheol. Acta*, **33**, 1 (1994).
20. E. Narimissa, V.H. Rolón-Garrido, and M.H. Wagner, Comparison between extensional rheological properties of low density polyethylene melt in SER and RME rheometric systems. NOVEL TRENDS IN RHEOLOGY VI, **1662** (2015), https://doi.org/10.1063/1.4918886.
21. M.H. Wagner, Korea-Australia Rheol. J., **11**, 293 (1999).
22. T.C.B. McLeish and R.G. Larson, J. Rheology, **42**, 1 (1998).
23. A. Bach, H.K. Rasmussen, and O. Hassager, *J. Rheol.*, **47**(2), 429 (2003).
24. H.K. Rasmussen, J.K. Nielsen, A. Bach, and O. Hassager, *J. Rheol.*, **49**, 2 (2005).
25. N.J. Alvarez, J.M.R. Marín, Q. Huang, M.L. Michelsen, and O. Hassager, *Physical review letters*, **110**, 16 (2013).
26. E. Torres, S.-W. Li, S. Costeux, and J.M. Dealy, *Journal of Rheology*, **59**, 5 (2015).
27. S. Costeux, P. Wood-Adams, and D. Beigzadeh, *Macromolecules*, **35**, 7 (2002).
28. M. Doi and S.F. Edwards, Dynamics of concentrated polymer systems. Part 3. The constitutive equation, Journal of the Chemical Society. *Journal of the Chemical Society, Faraday Transactions 2: Molecular and Chemical Physics*, **74**, 1818 (1978), https://doi.org/10.1039/F29787401818.
29. S. Pedersen and L.L. Chapoy, *J. Non-Newtonian Fluid Mech.*, **3**, 4 (1978).
30. H.M. Laun, *Rheol. Acta*, **17**, 1 (1978).
31. K. Osaki and M. Kurata, *Macromolecules*, **13**, 3 (1980).
32. C.M. Vrentas and W.W. Graessley, *J. Rheol.*, **26**, 4 (1982).
33. Y.H. Lim, *J. Rheol.*, **28**, 1 (1984).
34. S.L. Wingstrand, B. Shen, J.A. Kornfield, K. Mortensen, D. Parisi, D. Vlassopoulos, and O. Hassager, *ACS Macro Letters*, **6**, 11 (2017).